Competition between Auger Recombination and Hot-Carrier Trapping in PL Intensity Fluctuations of Type II Nanocrystals

*Benjamin D. Mangum, Feng Wang, Allison M. Dennis, Yongqian Gao, Xuedan Ma, Jennifer A. Hollingsworth, and Han Htoon**

***P**erforming time-tagged, time-correlated, single-photon-counting studies on individual colloidal nanocrystal quantum dots (NQDs), the evolution of photoluminescence (PL) intensity-fluctuation behaviors in near-infrared (NIR) emitting type II, InP/CdS core–shell NQDs is investigated as a function of shell thickness. It is observed that Auger recombination and hot-carrier trapping compete in defining the PL intensity-fluctuation behavior for NQDs with thin shells, whereas the role of hot-carrier trapping dominates for NQDs with thick shells. These studies further reveal the distinct ramifications of altering either the excitation fluence or repetition rate. Specifically, an increase in laser pump fluence results in the creation of additional hot-carrier traps. Alternately, higher repetition rates cause a saturation in hot-carrier traps, thus activating Auger-related PL fluctuations. Furthermore, it is shown that Auger recombination of negatively charged excitons is suppressed more strongly than that of positively charged excitons because of the asymmetry in the electron–hole confinement in type II NQDs. Thus, this study provides new understanding of how both NQD structure (shell thickness and carrier-separation characteristics) and excitation conditions can be used to tune the PL stability, with important implications for room-temperature single-photon generation. Specifically, the first non-blinking NQD capable of single-photon emission in the near-infrared spectral regime is described.*

Dr. B. D. Mangum,[+] Dr. F. Wang, Dr. A. M. Dennis,[++]
Dr. Y. Gao, Dr. X. Ma, Dr. J. A. Hollingsworth,
Dr. H. Htoon
Center for Integrated Nanotechnologies
Materials Physics, & Applications Division
Los Alamos National Laboratory
Los Alamos, New Mexico 87545, USA
E-mail: htoon@lanl.gov

[+]Present address: Pacific Light Technologies, Portland, Oregon, 97201, USA

[++]Present address: Departmentof Biomedical Engineering and Division of Materials Science and Engineering, Boston University, Boston, Massachusetts 02215 USA

BDM and FW contributed equally to this work

DOI: 10.1002/smll.201302896

1. Introduction

Chemically synthesized core/thick-shell nanocrystal quantum dots (NQDs),[1,2] which we have dubbed "giant" NQDs (g-NQDs) due to their relatively large size, are rapidly emerging as a new class of NQD possessing tremendous potential for applications, including bio-imaging/tracking,[3–6] solid-state lighting,[7,8] lasing,[9] and single/entangled-photon generation.[10,11] The prototype g-NQDs, (CdSe/CdS core/shell), have been repeatedly shown to afford unique and useful photophysical properties, including significant suppression of photoluminescence (PL) intermittency (blinking) and photo-bleaching[1,2,4,6,12] and more recently, fully non-blinking behavior,[13] along with environmentally independent quantum yields in emission[1,6] and highly efficient multiexciton emission.[14] The latter, at least, is directly tied to a strong

suppression of non-radiative Auger recombination (AR) that is also characteristic of these NQDs.[9,12,14–16] In addition, compared to standard NQDs (i.e., core only or core/thin-shell NQDs), the improved photostability of thick-shell CdSe/CdS NQDs has permitted studies that have revealed in detail the influence of the shell thickness on the electronic structure,[17] as well as the mechanisms responsible for the suppression of AR and blinking.[18–21] Furthermore, g-NQDs possess an enhanced solid-state performance[7] and minimal self-reabsorption,[8] which are key attributes for applications in, for example, solid-state lighting. However, CdSe/CdS g-NQDs are limited with respect to their spectral tunability, where core-size tuning yields wavelengths from about 610–685 nm,[13] in contrast with conventional core-only or thin-shell CdSe-based NQDs, which are well known for their ability to be tuned across the visible spectrum by simple core-size tuning.

Extending the non-blinking emission and AR suppression to other regimes of the electromagnetic spectrum is an essential step in realizing the potential of the g-NQD approach for a variety of technological applications. Particularly, g-NQDs capable of emitting in the near-infrared (NIR) could bring breakthroughs in biomedical imaging and laser media as well as single/entangled photon sources operating at telecommunication wavelengths. To this end, we recently synthesized a new g-NQD based on an InP core that was overcoated with a CdS shell of up to 10 monolayers (MLs) thick.[22] Non-blinking excitonic emission and a strong suppression of AR were observed for the first time in the NIR spectral range of 800–1300 nm from these new g-NQDs.[22,23]

In contrast to the well-studied CdSe/CdS g-NQDs, which are characterized by a quasi-type II energy-band alignment, InP/CdS g-NQDs are characterized by a pure type II band structure. In this case, electrons and holes are confined separately in the CdS shell and InP core of the core–shell structure, respectively.[22] Therefore, emission stems from the indirect recombination of an electron–hole pair across a staggered band alignment with its energy smaller than the bandgap of either the core or the shell component. Such "indirect emission" is known in the NQD literature,[24–26] and often affords near infrared PL.[27–32] However, prior to our study,[22] there have been no reports on type II emission properties at the single-NQD level because of rapid photo-bleaching and/or insufficiently bright emission, which are apparently "inherent" to these systems.[33] Unlike the earlier type II systems, the new InP/CdS NQD system afforded a highly stable PL, which provided a unique opportunity to investigate the influence of type II band alignment coupled with shell thickness on biexciton lifetimes and mechanisms responsible for blinking.[22]

Recently, we have shown that PL intensity fluctuations in a CdSe/CdS g-NQD system can occur via two distinct mechanisms, denoted as A-type and B-type blinking.[20] A-type blinking is characterized by the correlated fluctuation of PL intensity and lifetimes and is attributed to switching between neutral (X^0) and various negatively charged exciton states (e.g., X^-, X^{2-}), which have both a lower emission quantum yield (QY) and a faster PL decay due to AR.[34] The transition from the X^0 to the X^- and X^{2-} states in this process is believed to occur via the ejection of one or more holes through an AR event following NQD excitation to a bi-exciton (BX) or higher order multiexciton state.[34,35] B-type blinking on the other hand shows fluctuations only in the PL intensity, whereby the lifetime remains constant. We explained this phenomenon in terms of the trapping of hot electrons followed by a nonradiative recombination facilitated by surface defects.[20] Later, Qin et al. showed that B-type blinking can also occur via nonradiative recombination at deep hole traps created by surface oxidation following the photoionization of a hole.[36] However, for this model to be fully consistent with B-type blinking, the holes are required to be trapped prior to their relaxation to the lowest excitonic state (i.e., trapping of "hot holes"), as the trapping of holes after energy relaxation could introduce a fast component in the PL decay of the exciton similar to that observed in A-type blinking. Regardless, as the latter two processes differ mainly in the type of hot carrier (electron or hole), we refer to both of them here as 'hot-carrier trapping' processes.

In this work, we have investigated the influence of NQD structural factors, as well as the experimental conditions during NQD excitation, on whether AR or hot-carrier trapping processes dominate in determining the stability of NQD PL. Specifically, we have assessed the impact of shell thickness in the case of the fully type II InP/CdS system, coupled with experimental parameters, such as the pump fluence (i.e., energy per pulse per unit area) and repetition rate in single-dot time-tagged, time-correlated, single-photon-counting experiments. Significantly, we reveal specific combinations of shell thickness and excitation parameters that allow us to directly tune the balance of the two processes, with clear implications for the ultimate goal of achieving a perfectly stable near-IR single-photon emitter.

2. Results and Discussion

2.1. Influences of Shell Thickness on Suppression of PL Intensity Fluctuations

We first assessed the variation of PL intensity fluctuation characteristics for g-NQD samples of different shell thickness. To compare these properties at similar photo-generated electron-pair populations (in the order of 0.1), we adjusted the pump fluence of the laser excitation according to the volume of the g-NQDs. **Figure 1**a,b displays representative time traces for two g-NQDs together with the background threshold levels. Traces similar to these allow us to extract the "on" time fraction, or the fraction of time the g-NQD emits above a threshold background level. Data points for 70 g-NQDs plotted as a function of g-NQD shell thickness show a wide variation in the on-time fraction at all three shell thicknesses (Figure **1**c). However, the population fraction of g-NQDs showing strong blinking (on-time fraction <50%) decreases from around 40% to around 10% as the shell thickness is increased from 4 to 10 ML (blue data points). Correspondingly, the population fraction of the g-NQDs showing >70% on-time fraction increases with shell thickness (black data points). These findings are consistent with values reported in our previous study, which were based on 11 g-NQDs.[22]

The on-time fraction, however, is not enough to fully characterize the blinking property of these g-NQDs. For example, even among the g-NQDs showing a very high on-time

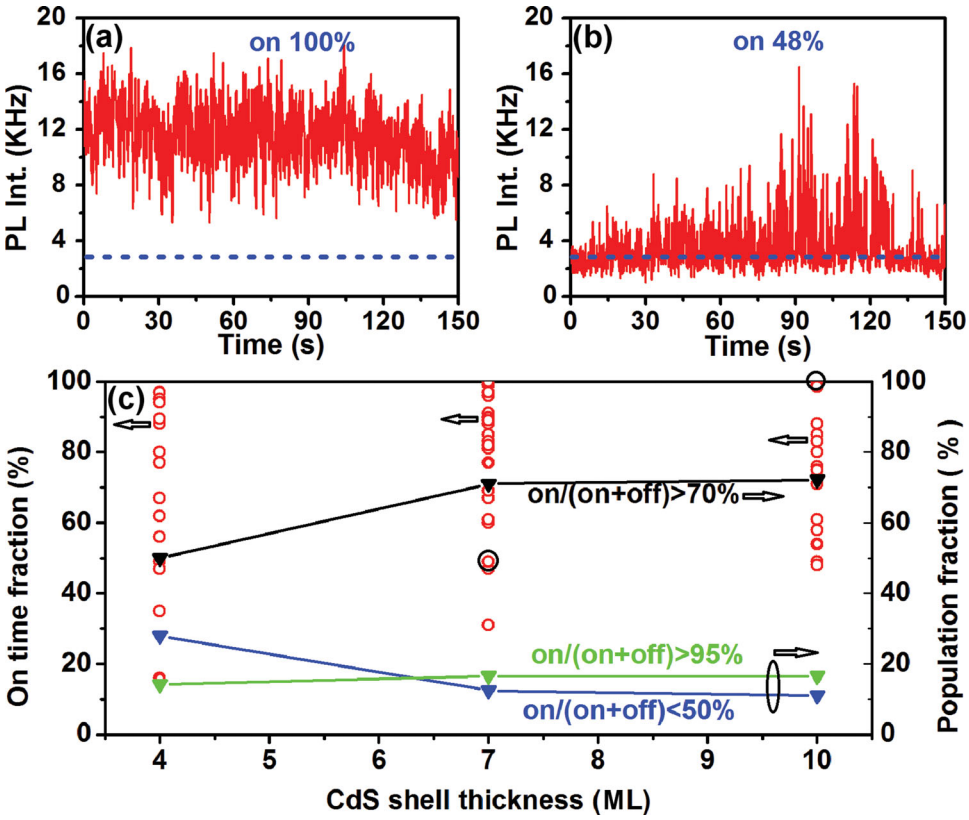

Figure 1. PL time traces of two g-NQDs that are "ON" for a) 100% and b) 48% of the time. c) On-time fraction of different g-NQDs plotted as a function of their shell thickness (red circles). The g-NQDs displayed in (a) and (b) are marked by black circles. The population fraction of g-NQDs with on-time fraction >95% (green triangles), >70% (black triangles) and <50% (blue trangles).

fraction, some showed a very stable PL emission with an intensity distribution approaching the Poissonian distribution of a shot-noise limited system, whereas others show a much wider intensity distribution. The PL time traces and intensity distribution histograms of two g-NQDs exemplifying this type of variation are displayed in **Figure 2**a–d. To further characterize this PL fluctuation behavior, we calculated the Mandel Q parameter, which provides a measure of the variation in PL intensity distribution from the Poissonian distribution for each PL time trace (i.e., $Q = (\langle n^2 \rangle - \langle n \rangle^2) / \langle n \rangle$, where n represents the number of PL counts measured within the 100 ms time bin),[37] and plotted its values in Figure 2e. The data show that although the population fraction of g-NQDs having a narrow intensity distribution approaching the Poissonian limit (i.e., Q<3: blue data points of Figure 2e) increases from 0% at 4 shell MLs to ca. 20% at 10 shell MLs, that of the g-NQDs with wide intensity distribution (Q>10 black data points of Figure 2e) decreases from 60% to 40%. These facts, together with the data displayed in Figure 1, highlight the benefits of a thick shell for suppressing the blinking in InP/CdS NQDs.

2.2. Strong Potential for Room-Temperature Single-Photon Generation

Although our g-NQDs display widely differing on-time fractions and Q values, our 2nd order photon-correlation ($g^{(2)}$) spectroscopy study reveals that all of our g-NQDs exhibit a very strong photon antibunching, signified by a near-complete disappearance of the center peaks in the $g^{(2)}$ functions. **Figure 3**a–c displays the $g^{(2)}$ functions of three different g-NQDs. The areas of the center peaks for these three g-NQDs as well as all the other g-NQD investigated are less than 5% of that of the side peaks. This very high degree of photon antibunching further indicates a very low probability of multi-exciton emission and therefore a high potential for room-temperature single-photon generation, which holds the key to realizing eavesdropping-proof quantum communication.[38,39] (The mechanism responsible for this low multi-exciton emission efficiency is discussed in the subsequent sections)

Although room-temperature single-photon generation has been observed before in standard core–shell NQDs,[40] these NQDs have never been considered seriously for these applications because of their rapid PL intensity fluctuations (blinking). However, the PL time traces of the representative g-NQDs (Figures 3d–f), as well as the statistics of Figure 2e, show that very stable, near-shot-noise limited PL emission (Q<3) with on-time fractions >95% is possible in about 20% of our g-NQD population. This population fraction can be improved toward unity through optimization of the shell growth as has been recently demonstrated in prototyped CdSe/CdS g-NQD systems.[13] Additionally, the emission of our type II g-NQDs already covers the telecommunication wavelength of 1.3 μm and should be extendable toward 1.5 μm,

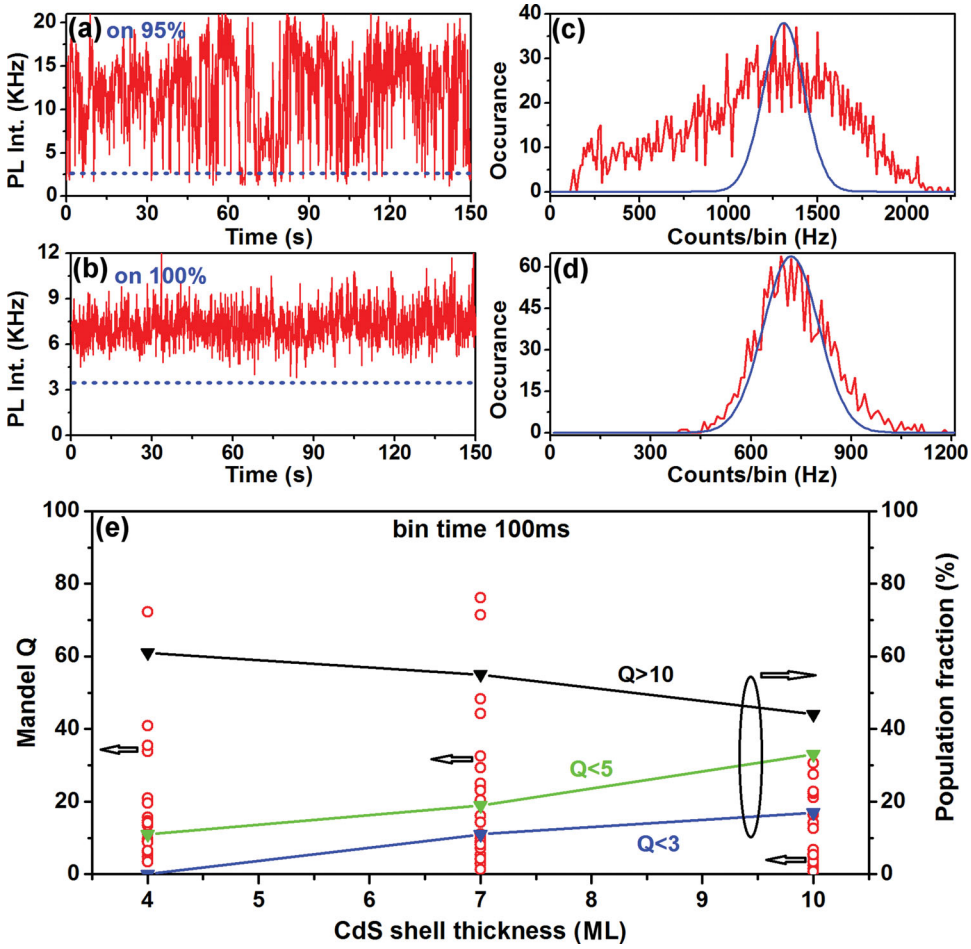

Figure 2. a,b) PL time traces of 2 g-NQDs that are on for more than 90% of the time and c,d) their PL intensity distributions (red trace) compared with the Poissonian distribution of detector shot noise (blue trace). e) Mandel Q parameters of different g-NQDs plotted as a function of their shell thickness (red circles). Population fraction of g-NQD with Q value >10 (black triangles), <5 (green triangles) and <3 blue trangles.

another telecommunication band, by tuning the g-NQD core-size and/or composition. Our g-NQDs therefore are endowed with a unique combination of fluctuation-free NIR PL emission and a low-multiexciton emission probability, both of which are ideally suited for room-temperature single-photon generation. Furthermore, our g-NQDs demonstrate a much greater potential benefit for single-photon source applications compared to a CdSe/CdS dot-in-rod system, which has recently been proposed for the same application based upon its ability to emit single photons and nonblinking PL in the red spectral range (ca. 600 nm).[41]

2.3. Competition between Auger Recombination and Hot-Carrier Trapping

2.3.1. Influence of Shell Thickness

We analyzed the fluorescence lifetime intensity distribution (FLID) maps of individual g-NQDs as a function of their shell thickness to assess the impact of shell thickness on the apparent competition between AR and hot-carrier trapping in blinking. In the case of A-type blinking, which is controlled by AR, the correlated fluctuation of the PL intensity and the lifetime gives rise to FLID maps that spread diagonally downward (**Figure 4**a). In the case of B-type blinking controlled by hot-carrier trapping, FLID maps spread vertically downward (Figure 4b). In Figure 4e, we plot the g-NQD population fractions for these two types together with those for g-NQDs showing both types of blinking (Figure 4c), as well as those for fluctuation-free g-NQDs (Figure 4d). The plot clearly indicates a decrease in the population fraction of g-NQDs showing A-type blinking, suggesting a lesser role of AR in blinking of thick-shell NQDs. We also observed an increase in the population fraction of NQDs showing B-type blinking. This increase, however, is accompanied by a decrease in the population showing both types of blinking (A+B). The sum of the NQD population fraction showing B-type alone and (A+B)-type remains constant for all shell thicknesses (76%, 72%, and 78% for 4, 7, and 10 shell layers, respectively). This fact suggests that the decrease in the A+B population is mainly the result from suppression of A-type blinking and more importantly, the influence of the B-type blinking remains nearly constant for all the shell thicknesses we investigated in this study. As the trapping of hot carriers in B-type blinking occurs at the surface defects, a thick shell providing better isolation of the carriers from the surface should in principle suppress B-type blinking. However, our prior study

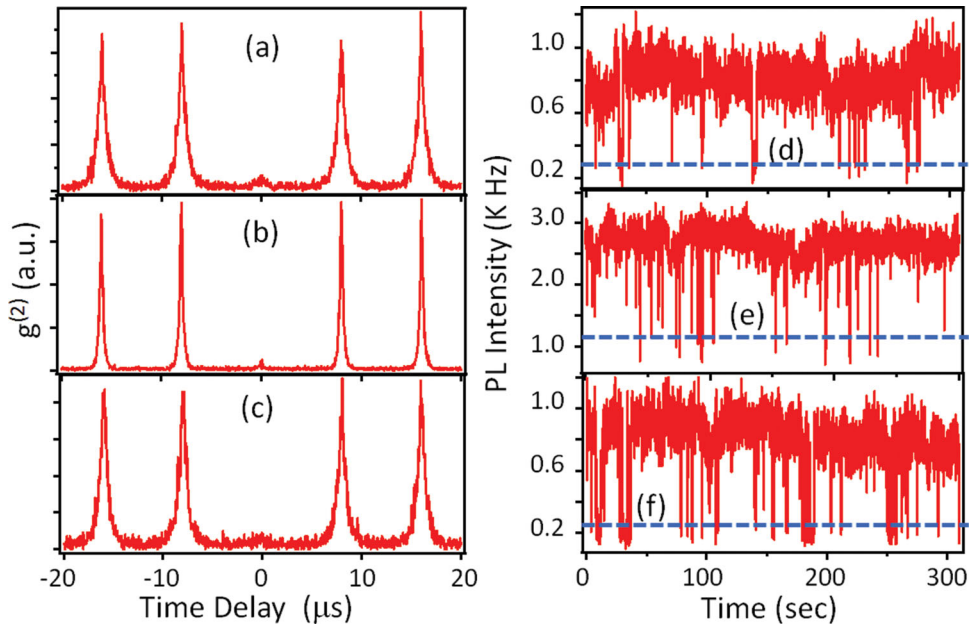

Figure 3. a–c) $g^{(2)}$ traces of three different g-NQDs showing near complete photon-antibunching. d–f) PL time traces of g-NQD shown in (a)–(c). The on-time fraction of all three g-NQD was >90%. The blue dotted line indicates the background level.

on CdSe/CdS g-NQDs revealed that this type of suppression required 12 ML or thicker shells.[20] As our InP/CdS g-NQDs in this study are coated with ≤10 ML-thick shells, it is perhaps not surprising that B-type blinking remains active. That said, as revealed in our prior ensemble-level time-resolved PL study,[22] such shell thicknesses are able to afford a nearly two order of magnitude suppression in the AR of BX. It is likely that a similarly strong suppression can also be expected for the AR of charged excitons, explaining the disappearance of A-type blinking with the increase in shell thickness up to 10 MLs.

2.3.2. Influence of Pump Power and Laser Repetition Rate

We further investigated the influence of the pump power and laser repetition rate on the competition between the AR and hot-carrier trapping processes in PL fluctuations. The pump dependence of the blinking traces and FLID maps of a g-NQD showing A-type blinking are displayed in **Figure 5**a,b and 5c,d respectively. As observed in earlier NQD blinking studies,[35,42–45] the g-NQDs blink more rapidly and the PL intensity distribution widens at higher pump powers because of an increase in photo-ionization probability. The decay of the total PL signal (black curve) at the highest pump power and the decay extracted for the highest and lowest PL intensity ranges marked in Figure 5d (i.e., 18–20 KHz (blue curve), 5–7 KHz (red curve), respectively) are displayed in Figure 5e. The fast-decay component observed in the 0–70 ns range (inset) of the total PL decay grows stronger with the laser pump power (not shown). It is therefore attributed to the decay of multiexciton states. Its decay constant of around 3.0 ns is also in reasonable agreement with the lifetime of BXs reported in our prior study. This fast component also appears in the decay curve extracted for the highest PL intensity range (blue curve), which can be fitted with a double exponential with time constants of 3.3 ns and 527 ns. We assigned the slower time constant of 527 ns to the radiative lifetime of the neutral exciton. The decay curve extracted for the lowest PL intensity can, however, be fitted with a triple exponential function yielding 2.0, 8.28, and 180 ns time constants with the two fast components being responsible for about 75% of the time-integrated PL signal. We believe that the decay of X^- is responsible for the slowest time constant of 180 ns, whereas the decays of the charged bi-exciton (BX^-) and other higher order charged excitons (X^{2-}, X^{3-}, etc.) combined together give rise to the two fast-decay components. Assigning these fast-decay components to a single specific process is not possible. Using the principle that a radiative lifetime of an X^- should be 2 times faster than that of a neutral exciton (i.e., $\tau_R^{x0} = 2\tau_R^{x^-}$),[19,46,47] and also understanding the relations between the lifetime and quantum yield (i.e., $1/\tau^{x^-} = 1/\tau_{Auger}^{x^-} + 1/\tau_R^{x^-}$ and $QY_{x^-} = \tau_R^{x^-}/\tau^{x^-}$),[19,47,48] we can estimate QY_{x^-} to be 70% for τ^{x^-} and τ_R^{x0} of 180 ns and 527 ns respectively. This high QY_{x^-} value further indicates a suppression in the AR of the X^- state. The observed PL intensity of a low-emissive state, however, is decreased due to the contribution of higher order charged excitons and biexcitons, which are expected to have a much lower quantum yield.[49]

Similar to the case of CdSe/CdS g-NQDs,[10,11,18] X^0 state lifetimes of our g-NQDs are observed to vary widely in the range of 100 to 550 ns regardless of their shell thickness. Due to this wide variation, X^- state lifetimes are also distributed widely, from 50 to 200 ns. As a result we were not able to establish a meaningful correlation between the X^- lifetimes and the shell thickness. Nevertheless, these very long X^- lifetimes suggest that the AR is somewhat suppressed for negatively charged excitons. On the other hand, our previous ensemble-level time-resolved PL (TRPL) study revealed that although the AR of BX in thick-shell (10 ML) samples is strongly suppressed compared to that of the thin-shell

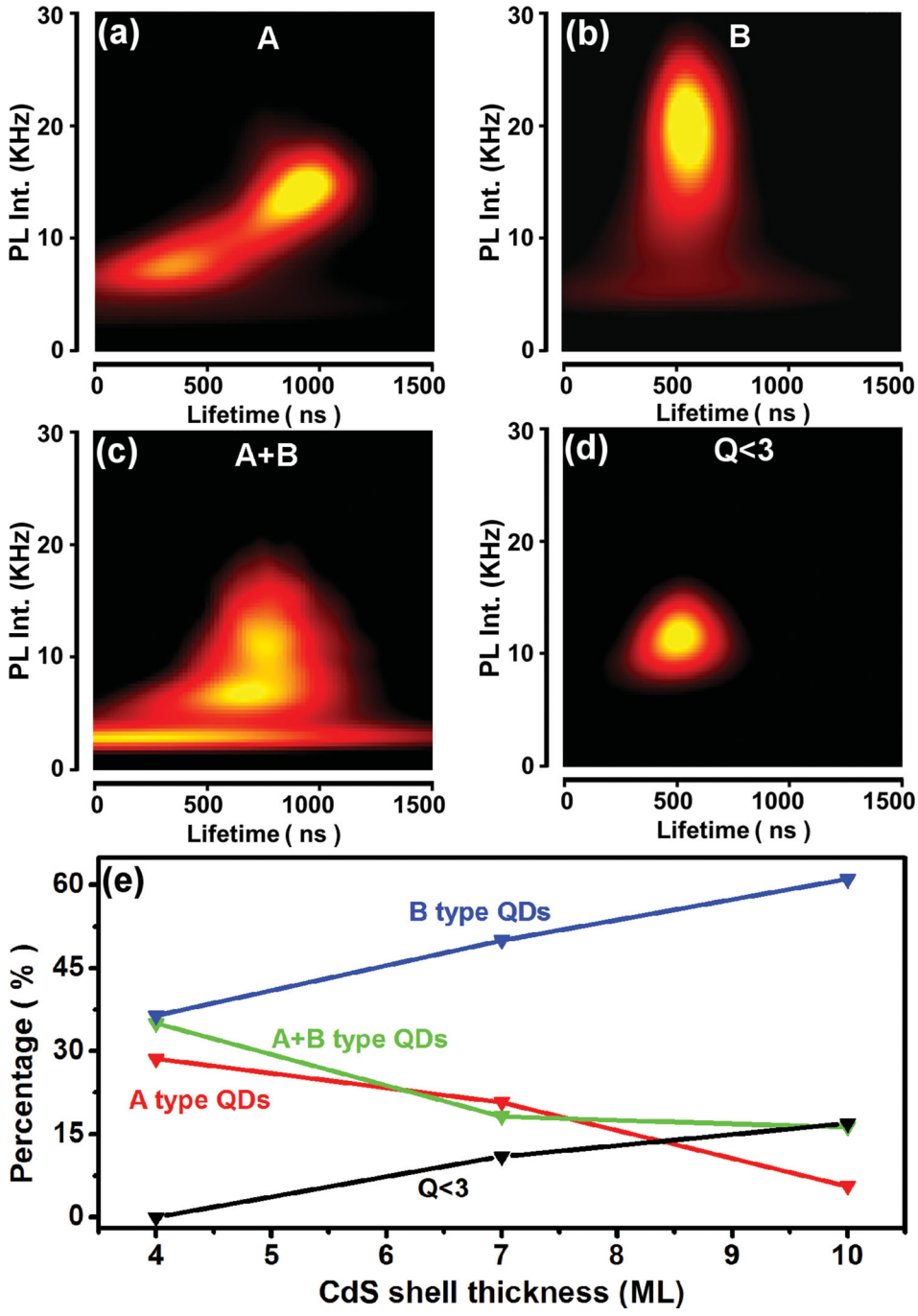

Figure 4. FLID maps of 4 different g-NQDs showing a) A-type blinking, b) B-type blinking, c) both types of blinking, and d) complete suppression of intensity fluctuation. e) Population fraction of g-NQDs exhibiting A-type blinking (red triangles), B-type blinking (blue triangles), both types of blinking (green triangles), and complete suppression of blinking characterized by Q values less than 3 (black triangles).

(4 ML) sample, the BX lifetime of the thickest shell (10 ML) samples is observed to be only 7 ns, which is significantly shorter compared to the lifetimes of the X^0 and X^- states. In accordance with this lifetime our quantum-yield measurement for the BXs via 2nd order photon-correlation spectroscopy[12,16,18,50] yielded a very strong photon anti-bunching (Figure 3a-c) corresponding to very low BX QY values of <5% for almost all the g-NQDs we have investigated. These facts suggest that AR is not as suppressed in BX as it is in X^-. Because the AR rate of BX is defined by the sum of the AR rates of the negatively and positively charged excitons (i.e., $\Gamma_{BX,A} = 2\,\Gamma_{X^-,A} + 2\,\Gamma_{X^+,A}$),[19,47,48] we conclude that although the AR of the X^- state may somewhat be suppressed, the AR of the X^+ state remains strong and defines the decay rate and low QY of the BX state. The existence of such asymmetry in AR processes have been reported in several prior studies[19,47] and attributed, in the case of CdSe/CdS g-NQDs, to the asymmetry in the band offset of the CdSe/CdS system, which allows partial delocalization of the electrons to the thick shell whereas holes are strongly

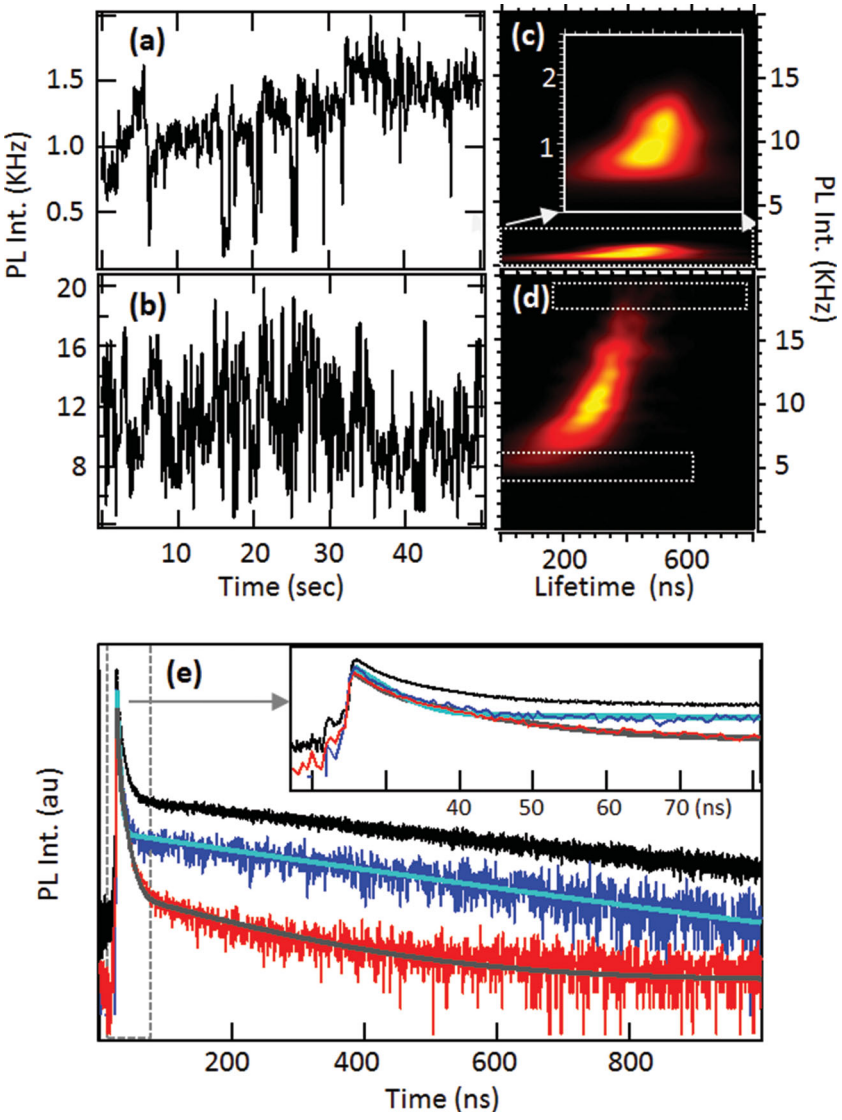

Figure 5. a,b) PL time traces and c,d) FLID maps of a single g-NQD taken at the relative pump fluences of 0.1 (a,c) and 1.0 (b,d). e) PL decay curves of the total PL signal (black trace) and high (blue) and low (red) PL emission ranges marked with dotted lines in (d). Light blue and gray traces are the double and triple exponential fits for the respective decay curves. Inset: Expanded view of the first 80 ns of the main plot.

localized in the core.[19] As the type II band alignment of our InP/CdS system further accentuates this carrier-separation effect, a stronger asymmetry in AR is indeed expected in our system.

In B-type blinking, hot-carrier trapping is followed by the non-radiative recombination of the trapped carrier with the opposite carrier left behind in the core of the NQD. When the carriers are photo-generated at a very high rate, the traps can be filled at a rate faster than the rate of this non-radiative recombination process. This can lead to the saturation of available hot-carrier traps and suppression of B-type blinking. At that stage, the probability of populating the lowest emitting state with BX will increase and A-type blinking will become active when the AR of the BX leads to charging of the g-NQD. This dramatic transition from B-type to A-type blinking is observed when the repetition rate of the laser excitation is increased whereby the pump fluence is kept constant. A representative data set is shown in **Figure 6**. At the low repetition rate of 200 kHz, the FLID of Figure 6b shows a vertical spread of distribution around the average decay rate of 400 ns indicating B-type blinking. Whereas the FLID of Figure 6d taken on the same g-NQD but at a repetition rate of 400 kHz shows a diagonal distribution with around 400 ns and <200 ns for the highest and lowest PL emission levels, respectively. This correlated fluctuation of the intensity and lifetime points to a suppression of B-type blinking and an emergence of A-type blinking. At this repetition rate, the pulse to pulse separation of 2.5 μs is longer than the 400 ns average PL lifetime of the g-NQD by a factor of 6, and allows complete relaxation of the exciton population to the ground state. The BXs responsible for charging of the g-NQD via their AR are, therefore, not formed in two successive excitations but are created by a single laser pulse. Although the probability of generating two excitons depends only on the pump fluence, which remains constant for the two repetition rates in this experiment, BXs cannot be formed efficiently at the low repetition rate because of hot-carrier trapping. Their formation becomes efficient enough to activate A-type blinking only after saturation of the traps at the high repetition rate.

As both the repetition rate (R) and pump fluence (f) contribute equally to the exciton generation rate as $\sigma \cdot f \cdot R$ where σ is the absorption cross section of the g-NQD, it is reasonable to expect a similar B-type to A-type transition with an increase in pump fluence. On the contrary, we observed that B-type blinking is maintained over more than one order of magnitude change in pump power, whereas the blinking becomes more rapid and the intensity fluctuation range widens. The pump-dependent evolution of the PL time traces and FLID maps demonstrating this behavior are displayed in **Figure 7**a–f. The PL time traces show that blinking becomes more rapid and the range of intensity fluctuation (i.e., PL_{max} –PL_{min}) widens from around 1 KHz to more than 5 KHz as the pump fluence is increased by more than one order of magnitude. The FLID maps (Figure 7e,f), on the other hand, spread only in the vertical direction keeping the distribution of lifetimes essentially unchanged in the 250–350 ns range (white dashed lines). These data confirm that no charge-fluctuation-related lifetime fluctuations were introduced and B-type blinking strengthens with an increase in pump fluence.

NANO MICRO small

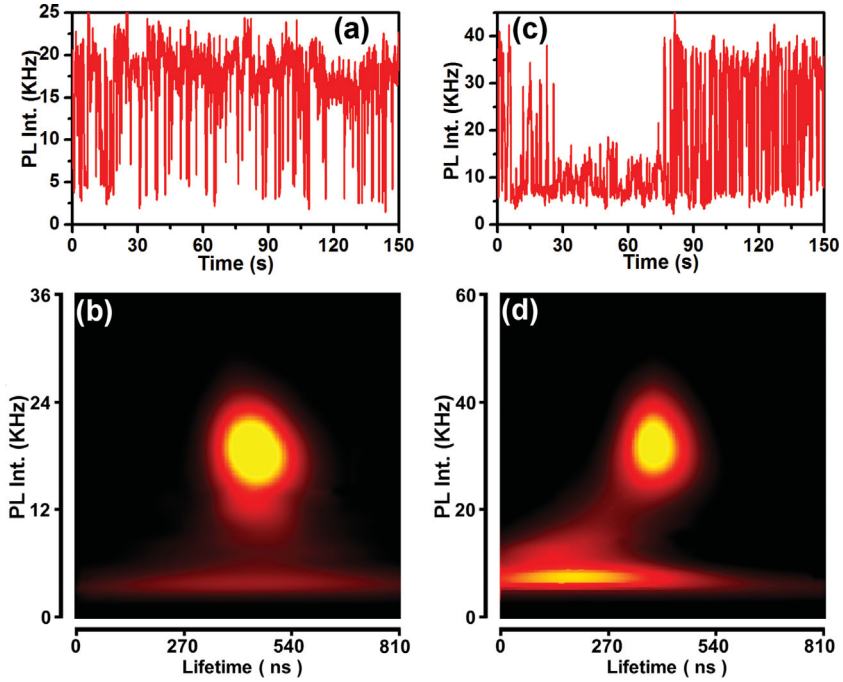

Figure 6. PL time traces (a,c) and FLID maps (b,d) of a single g-NQD acquired at the laser repetition rates of 200 KHz for (a,b) and 400 KHz for (c,d).

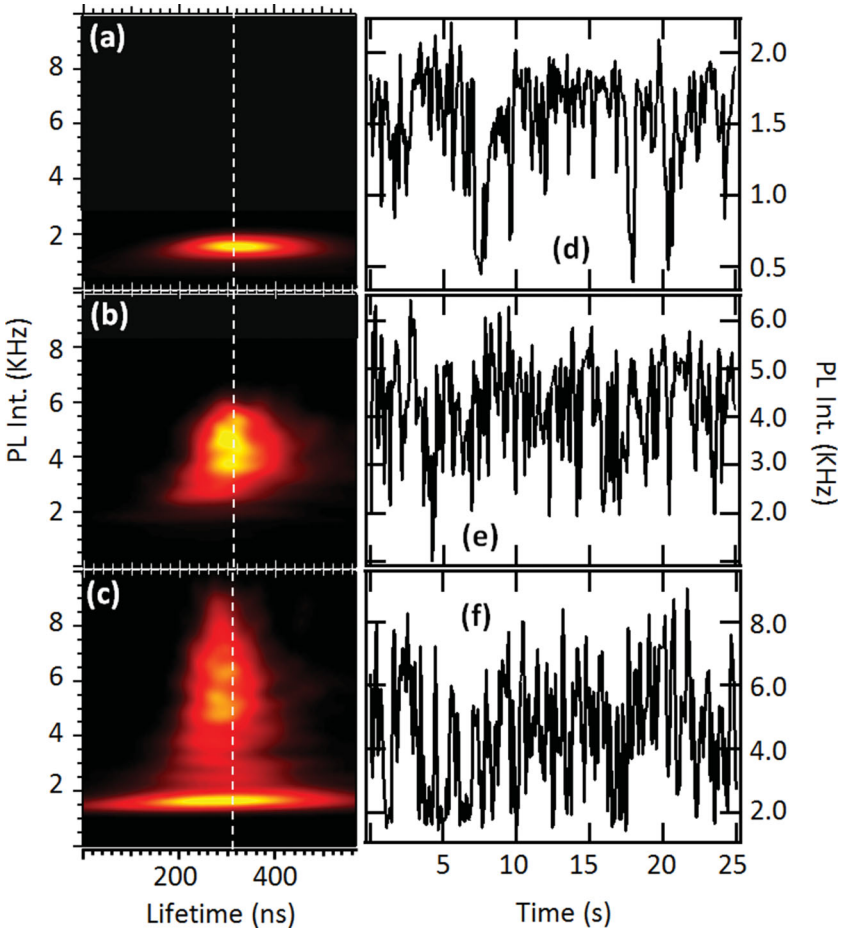

Figure 7. FLID maps (a–c) and PL time traces (d–f) of a single g-NQD acquire at 3 different relative pump fluences of a) 0.1, b) 0.3, and c) 1.0. These data sets were selected out of 12 pump-dependent measurements performed on a single g-NQD at the repetition rate of 200 KHz.

3. Conclusions and Summary

Our findings suggest that although excitation at higher repetition rates can lead to a saturation of hot-carrier traps, an increase in pump fluence generates more hot-carrier traps. This may result from photo-induced desorption or destruction of ligand molecules that passivate the surface of the g-NQDs. However, such a destruction of the ligand shell usually leads to permanent photobleaching rather than a reversible increase and decrease of the blinking as we have observed here. Very recently, theoretical studies of O. Voznyy et al. have revealed that surface traps can be formed not only during NQD growth, but they can also occur dynamically in a fully formed NQD in response to a variation in carrier population in a band.[51] The study further pointed out that such a variation can be triggered by photo-excitation. This dynamical trap formation can therefore explain our observations. Additionally, in the deep-hole trap model, which W. Qin et al. proposed to explain B-type blinking, the formation of deep traps are initiated by the photoionization of a hole in the BX AR,[36] therefore an increase of the pump fluence can give rise to the creation of more deep traps.

In summary, our study reveals that although AR and hot-carrier trapping compete in defining the PL-intensity fluctuation behavior of our type-II g-NQDs with thin shells, the role of AR diminishes and that of hot-carrier trapping becomes more dominant with increasing shell thickness. Exciting the g-NQD at a higher repetition rate saturates the hot-carrier traps and suppresses B-type blinking. This process makes g-NQDs more prone to photo-induced charging and enhances the likelihood of A-type blinking. In contrast, we observe that an increase in pump power strengthens B-type blinking through the creation of more hot-carrier traps. We tentatively attribute the dynamical formation of traps and Auger-induced formation of deep-hole traps as possible mechanisms for the photo-generation of hot-carrier traps. In addition to these insights into the PL-intensity fluctuation processes, our study reveals several benefits of thick shells in achieving the complete suppression of PL-intensity fluctuations in NIR emitting, type-II NQDs.

4. Experimental Section

Synthesis of InP/CdS Core–Shell g-NQDs: A detailed procedure for the synthesis of InP/CdS core–shell g-NQDs was provided in our prior publication.[22] Briefly, we first synthesized InP cores from indium myristate and tris(trimethylsilyl)phosphine [$(TMS)_3P$] in octadecene (ODE) and oleylamine solutions by adapting the procedure reported by R. Xie et al.[52] Taking care to avoid exposure to air and light prior to shell growth, CdS shells were then added using a modified successive ionic layer adsorption and reaction (SILAR) approach. Cadmium oleate in oleic acid (0.2 M $Cd(OA)_2$, 1:4 Cd/OA) and sulfur in ODE (0.2 M) comprised the cation and anion precursor solutions, respectively. To avoid etching of the InP cores, the first shell monolayer was added at a lower temperature compared to subsequent monolayer additions (150 °C compared to 240 °C, respectively). After addition of the first, "protective" monolayer, the higher reaction temperature allowed the growth of a high-quality thick shell, which was also supported by long annealing times of around 2.5 h following each addition of $Cd(OA)_2$ and around 1 h following each addition of sulfur. Large samples of the reaction solution were taken after 1, 4, 7, and 10 shells and stored "raw", i.e., in the reaction solution, at 4 °C. Such raw samples could be worked up and analyzed as being "fresh" even months after the synthesis was completed without compromising on the sample quality. The size of the resulting NQDs was determined by the analysis of transmission electron microscopy (TEM) images for hundreds of dots. A JEOL 2010 operating at 200 kV was used to perform the TEM studies.

Single NQD Time-Tagged, Time-Correlated PL Experiments: A home-built laser scanning confocal microscope equipped with a 1.3 NA, 100× oil immersion objective was used to perform single-dot spectroscopy. g-NQDs were sparsely dispersed on a coverslip with a concentration of roughly 1 g-NQD per 5 square micrometers area. A 405 nm ps diode laser was focused to a diffraction limited spot (ca. 300-nm diameter) to excite the g-NQDs. The PL signal was directed to 2 avalanched photo diodes (APDs) forming a Hanbury-Brown-Twiss spectrometer. PL-intensity time traces, fluorescence lifetime-intensity distributions (FLIDs), and 2^{nd} order photon-correlation traces were collected simultaneously using Picoquant Hydra-Harp time-correlated photon-counting electronics and custom-made analysis software. Our APDs allowed us to detect PL emission down to 950 nm covering more than 40% of the total emission spectrum (800–1300 nm). When the time-resolved PL experiments on our g-NQD films were performed using a photomultiplier tube (PMT) with InGaAs cathode that was sensitive down to 1400 nm, we observed decay curves that were nearly identical to those measured with our APDs.[22] This fact suggests that the PL-decay dynamics and emission characteristics of our g-NQDs do not vary across the broad emission spectrum and therefore the use of APDs with a limited detection range was sufficient.

Supporting Information

Supporting Information is available from the Wiley Online Library or from the author.

Acknowledgements

This work was mainly supported by a Single-Investigator Small-Group Research Award (2009LANL1096), Office of Basic Energy Sciences (OBES), Office of Science (OS), U.S. Department of Energy (DOE), and was conducted at the Center for Integrated Nanotechnologies, a DOE, OS, OBES user facility and nanoscale science research center. J.A.H acknowledges partial support by NIH-NIGMS Grant 1R01GM084702–01.

[1] Y. Chen, J. Vela, H. Htoon, J. L. Casson, D. J. Werder, D. A. Bussian, V. I. Klimov, J. A. Hollingsworth, *J. Am. Chem. Soc.* **2008**, *130*(15), 5026–5027.
[2] B. Mahler, P. Spinicelli, S. Buil, X. Quelin, J.-P. Hermier, B. Dubertret, *Nat. Mater.* **2008**, *7*(8), 659–664.
[3] J. A. Hollingsworth, J. Vela, C. Yongfen, H. Htoon, V. I. Klimov, A. R. Casson, *Proc. SPIE* **2009**, 718904, 7.
[4] P. Spinicelli, B. Mahler, S. Buil, X. Quelin, B. Dubertret, J.-P. Hermier, *ChemPhysChem* **2009**, *10*(6), 879–882.
[5] K. Marchuk, Y. Guo, W. Sun, J. Vela, N. Fang, *J. Am. Chem. Soc.* **2012**, *134*(14), 6108–6111.
[6] J. Vela, H. Htoon, Y. F. Chen, Y. S. Park, Y. Ghosh, P. M. Goodwin, J. H. Werner, N. P. Wells, J. L. Casson, J. A. Hollingsworth, *J. Biophotonics* **2010**, *3*(10–11), 706–717.
[7] B. N. Pal, Y. Ghosh, S. Brovelli, R. Laocharoensuk, V. I. Klimov, J. A. Hollingsworth, H. Htoon, *Nano Lett.* **2011**, *12*(1), 331–336.
[8] J. Kundu, Y. Ghosh, A. M. Dennis, H. Htoon, J. A. Hollingsworth, *Nano Lett.* **2012**, *12*(6), 3031–3037.
[9] F. García-Santamaría, Y. Chen, J. Vela, R. D. Schaller, J. A. Hollingsworth, V. I. Klimov, *Nano Lett.* **2009**, *9*(10), 3482–3488.
[10] Y.-S. Park, Y. Ghosh, Y. Chen, A. Piryatinski, P. Xu, N. H. Mack, H.-L. Wang, V. I. Klimov, J. A. Hollingsworth, H. Htoon, *Phys. Rev. Lett.* **2013**, *110*, 117 401.
[11] Y.-S. Park, Y. Ghosh, P. Xu, N. H. Mack, H.-L. Wang, J. A. Hollingsworth, H. Htoon, *J. Phys. Chem. Lett.* **2013**, *4*, 1465–1470.
[12] O. Chen, J. Zhao, V. P. Chauhan, J. Cui, C. Wong, D. K. Harris, H. Wei, H.-S. Han, D. Fukumura, R. K. Jain, M. G. Bawendi, *Nat. Mater.* **2013**, *12*(5), 445–451.
[13] Y. Ghosh, B. D. Mangum, J. L. Casson, D. J. Williams, H. Htoon, J. A. Williams, *J. Am. Chem. Soc.* **2012**, *134*(23), 9634–9643.
[14] H. Htoon, A. V. Malko, D. Bussian, J. Vela, Y. Chen, J. A. Hollingsworth, V. I. Klimov, *Nano Lett.* **2010**, *10*(7), 2401–2407.
[15] P. Spinicelli, S. Buil, X. Quelin, B. Mahler, B. Dubertret, J. P. Hermier, *Phys. Rev. Lett.* **2009**, *102*(13), 136 801.
[16] J. Zhao, O. Chen, D. B. Strasfeld, M. G. Bawendi, *Nano Lett.* **2012**, *12*(9), 4477–4483.
[17] S. Brovelli, R. D. Schaller, S. A. Crooker, F. Garcia-Santamaria, Y. Chen, R. Viswanatha, J. A. Hollingsworth, H. Htoon, V. I. Klimov, *Nat. Commun.* **2011**, *2*, 280.
[18] Y. S. Park, A. V. Malko, J. Vela, Y. Chen, Y. Ghosh, F. Garcia-Santamaria, J. A. Hollingsworth, V. I. Klimov, H. Htoon, *Phys. Rev. Lett.* **2011**, *106*(18), 187 401.
[19] C. Galland, Y. Ghosh, A. Steinbrück, J. A. Hollingsworth, H. Htoon, V. I. Klimov, *Nat. Commun.* **2012**, *3*, 908.
[20] C. Galland, Y. Ghosh, A. Steinbrück, M. Sykora, J. A. Hollingsworth, V. I. Klimov, H. Htoon, *Nature* **2011**, *479*(7372), 203–207.
[21] C. Javaux, B. Mahler, B. Dubertret, A. Shabaev, A. V. Rodina, A. L. Efros, D. R. Yakovlev, F. Liu, M. Bayer, G. Camps, L. Biadala, S. Buil, X. Quelin, J. P. Hermier, *Nat. Nanotechnol.* **2013**, *8*(3), 206–212.

[22] A. M. Dennis, B. D. Mangum, A. Piryatinski, Y.-S. Park, D. C. Hannah, J. L. Casson, D. J. Williams, R. D. Schaller, H. Htoon, J. A. Hollingsworth, *Nano Lett.* **2012**, *12*(11), 5545–5551.
[23] This very broad emission results from the type II nature of the optical transition. Our single-dot PL spectra indeed show an equally broad emission spectrum (Supporting Information, Figure S2). TEM study of our sample also reveals a narrow size distribution of 5.24 ± 0.56 nm for 4ML, 6.84 ± 0.68 nm for 7ML, and 8.3 ± 0.72 nm for 10ML g-NQD samples, respectively (Supporting Information, Figure S3).
[24] K. Yu, B. Zaman, S. Romanova, D. S. Wang, J. A. Ripmeester, *Small* **2005**, *1*(3), 332–338.
[25] P. T. K. Casson, C. d. M. Donega, S. S. van Bavel, S. C. J. Meskers, N. A. J. M. Sommerdijk, R. A. J. Janssen, *J. Am. Chem. Soc.* **2007**, *129*(48), 14 880–14 886.
[26] V. I. Klimov, S. A. Ivanov, J. Nanda, M. Achermann, I. Bezel, J. A. McGuire, A. Piryatinski, *Nature* **2007**, *447*(7143), 441–446.
[27] B. Blackman, D. Battaglia, X. Peng, *Chem. Mater.* **2008**, *20*(15), 4847–4853.
[28] W. Zhang, G. Chen, J. Wang, B.-C. Ye, X. Zhong, *Inorg. Chem.* **2009**, *48*(20), 9723–9731.
[29] X. Li, H. Shen, S. Li, J. Z. Niu, H. Wang, L. S. Li, *J. Mater. Chem.* **2010**, *20*(5), 923–928.
[30] A. Narayanaswamy, L. F. Feiner, A. Meijerink, P. J. van der Zaag, *ACS Nano* **2009**, *3*(9), 2539–2546.
[31] L. Li, P. Reiss, *J. Am. Chem. Soc.* **2008**, *130*(35), 11 588–11 589.
[32] M. R. Kim, J. H. Chung, M. Lee, S. Lee, D.-J. Fang, *J. Colloid Interface Sci.* **2010**, *350*(1), 5–9.
[33] B. Chon, S. J. Lim, W. Kim, J. Seo, H. Kang, T. Joo, J. Hwang, S. K. Shin, *Phys. Chem. Chem. Phys.* **2010**, *12*(32), 9312–9319.
[34] A. L. Efros, M. Rosen, *Phys. Rev. Lett.* **1997**, *78*(6), 1110–1113.
[35] J. J. Peterson, D. J. Nesbitt, *Nano Lett.* **2009**, *9*(1), 338–345.
[36] W. Qin, P. Guyot-Sionnest, *ACS Nano* **2012**, *6*(10), 9125–9132.
[37] G. Margolin, V. Protasenko, M. Kuno, E. Barkai, *J. Phys. Chem. B* **2006**, *110*(38), 19 053–19 060.
[38] C. H. Bennett, G. Brassard, A. K. Ekert, *Sci. Am.* **1992**, *267*(4), 50–57.
[39] C. H. Bennett, D. P. DiVincenzo, *Nature* **2000**, *404*(6775), 247–255.
[40] P. Michler, A. Imamoglu, M. D. Mason, P. J. Carson, G. F. Strouse, S. K. Buratto, *Nature* **2000**, *406*(6799), 968–970.
[41] F. Pisanello, G. Lemenager, L. Martiradonna, L. Carbone, S. Vezzoli, P. Desfonds, P. D. Cozzoli, J.-P. Hermier, E. Giacobino, R. Cingolani, M. De Vittorio, A. Bramati, *Adv. Mater.* **2013**, *25*(14), 1974–1980.
[42] A. V. Malko, Y. S. Park, S. Sampat, C. Galland, J. Vela, Y. Chen, J. A. Hollingsworth, V. I. Klimov, H. Htoon, *Nano Lett.* **2011**, *11*(12), 5213–5218.
[43] A. A. Cordones, T. J. Bixby, S. R. Leone, *J. Phys. Chem. C* **2011**, *115*(14), 6341–6349.
[44] P. A. Frantsuzov, S. Volkan-Kacso, B. Janko, *Nano Lett.* **2013**, *13*(2), 402–408.
[45] K. Zhang, H. Chang, A. Fu, A. P. Alivisatos, H. Yang, *Nano Lett.* **2006**, *6*(4), 843–847.
[46] P. P. Jha, P. Guyot-Sionnest, *J. Phys. Chem. C* **2007**, *111*(42), 15 440–15 445.
[47] P. P. Jha, P. Guyot-Sionnest, *ACS Nano* **2009**, *3*(4), 1011–1015.
[48] P. P. Jha, P. Guyot-Sionnest, *J. Phys. Chem. C* **2010**, *114*(49), 21 138–21 141.
[49] J. Zhao, G. Nair, B. R. Fisher, M. G. Bawendi, *Phys. Rev. Lett.* **2010**, *104*(15), 157 403.
[50] G. Nair, J. Zhao, M. G. Bawendi, *Nano Lett.* **2011**, *11*(3), 1136–1140.
[51] O. Voznyy, S. M. Thon, A. H. Ip, E. H. Sargent, *J. Phys. Chem. Lett.* **2013**, *4*(6), 987–992.
[52] R. Xie, D. Battaglia, X. Peng, *J. Am. Chem. Soc.* **2007**, *129*(50), 15 432–15 433.

Received: September 6, 2013
Revised: February 18, 2014
Published online: April 9, 2014

